A Comparative Study of Li-ion Battery Models and Nonlinear Dual Estimation Strategies

M. S. Farag[1], R. Ahmed[1], S. A. Gadsden[1], S. R. Habibi[1], and J. Tjong[2]
[1]McMaster University, Hamilton, Ontario, Canada and [2]Ford Canada
E-mail: mohammed.farag@mcmaster.ca

***Abstract*-Due to their high energy density, durability, low cost, and inherent safety, lithium-ion (Li-ion) batteries are quickly becoming the most popular energy storage method for electric vehicles. Difficulty arises in properly modeling these types of batteries due to a large number of parameters and different architectures. This paper looks at studying six different Li-ion battery models found in literature, and compares their relative performance based on a benchmark dataset. Kalman-based filtering strategies are also employed to estimate important battery parameters such as capacitance, hysteresis, and state of charge (SOC). In addition, the relatively new smooth variable structure filter (SVSF) is used and compared with these Kalman-based strategies.**

INTRODUCTION

A variety of batteries have been studied in literature, most notably lead-acid and lithium-ion (Li-ion) batteries [1, 2, 3, 4, 5]. Lead-acid batteries are the oldest type of rechargeable batteries, and are most commonly found in motor vehicles. Lithium-ion batteries are also a form of rechargeable battery, which contain lithium in its positive electrode (cathode). These batteries are usually found in portable consumer electronics (i.e., laptops or notebooks) due to particularly high energy-to-weight ratios, slow self-discharge, and a lack of memory effect (i.e., where a battery loses its maximum energy capacity over time) [2]. In recent years, Li-ion batteries have slowly entered the hybrid electric vehicle market, due to the fact that they offer better energy density compared to standard batteries [6].

Difficulty arises in properly modeling these types of batteries due to a large number of parameters and different architectures. A significant amount of research has been performed on battery management systems, with excellent surveys found in [2, 7, 8, 9, 10]. Battery management systems estimate important parameters which affect the operating condition of the batteries or pack of batteries [7]. These parameters typically include the following: battery state of charge (SOC), power fade, cpacity fade, and instantaneous available power [7]. However, these values are not known exactly and they must be estimated from available measurements (e.g., voltages). Observations of the system are made through the use of sensors which contain information on the variables of interest. Filters are ued to remove unwanted components such as noise (system or measurement) from the observations in an effort to provide accurate estimates of the states or parameters [11].

Advanced filtering and estimation methods such as the Kalman filter (KF) or smooth variable structure filter (SVSF) may be used to estimate these values. Most estimators are model-based, and as such are sensitive to modeling uncertainties and errors. Therefore, implementing accurate system models is extremely important for obtaining correct state and parameter estimates.

The purpose of this paper is to compare the performances of some of the most popular Li-ion battery models found in literature [7]. A benchmark dataset is used to study the effectiveness of these models, in conjunction with implementing Kalman-based filters and the smooth variable structure filter (SVSF). The following section describes the battery models in more detail, and are as presented in [7]. Section III provides an overview of the estimation methods. The main simulation results are shown in Section IV, followed by a brief discussion. Section V concluldes the main findings of this paper.

BATTERY MODELS

A. Combined Model

The terminal voltage of the battery may be predicted in a number of different ways. One important method of predicting the voltage is based on the SOC. A number of models have been formulated and are adapted in [7] and [12]. The following three are among the most popular combined models [7]:

- Shepherd: $y_k = E_0 - Ri_k - K_i/z_k$
- Unnewehr universal model: $y_k = E_0 - Ri_k - K_i z_k$
- Nernst: $y_k = E_0 - Ri_k + K_2 \ln(z_k) + K_3 \ln(1 - z_k)$

In these models, y_k is the cell terminal voltage, R is the cell internal resistance (different values may be used for charge/discharge at different SOC levels), K_i is the polarization resistance, and $K_\#$ are constants chosen to make the model fit the data [7]. Note that all of these models may be collected to make a 'combined model' that performs better than any of the individual models alone [7]. The combined model is defined by the following [7]:

$$z_{k+1} = z_k - \left(\frac{\eta_i \Delta t}{C}\right) i_k \tag{2.1.1}$$

$$y_k = K_0 - Ri_k - \frac{K_1}{z_k} - K_2 z_k + K_3 \ln(z_k) + K_4 \ln(1 - z_k) \tag{2.1.2}$$

This model has the advantage of being linear in the parameters, which makes it easier to implement and estimate.

978-1-4673-1408-4/12/$31.00 ©2012 IEEE

Accordingly, the unknown qunaities in the model may be estimated using a system identification procedure [7]. For example, given a set of N cell input-output parameters (y_k, i_k, z_k), the values may be solved for in a closed form using least squares estimation [7].

B. Simple Model

As presented in [7], for further insight, one can evaluate the parameter values fit to the combined model (presented earlier). The model output equation may be divided into two additive parts: one depending only on the SOC, and the other depending only on the current. Doing so yields:

$$f(z_k) = K_0 - \frac{K_1}{z_k} - K_2 z_k + K_3 \ln(z_k) + K_4 \ln(1 - z_k) \quad (2.2.1)$$

$$f(i_k) = R i_k \quad (2.2.2)$$

As explained in [7], an easier and more accurate implementation of the combined model is as follows:

$$z_{k+1} = z_k - \left(\frac{\eta_i \Delta t}{C}\right) i_k \quad (2.2.3)$$

$$y_k = OCV(z_k) - R i_k \quad (2.2.4)$$

Where OCV refers to the open circuit voltage.

C. Zero-State Hysteresis Model

An important concept that is overlooked by the previous two models includes hysteresis. For improved SOC estimation, the hysteresis effects of the terminal voltage should be considered [7]. As described in [7], a basic model of hysteresis simply adds a term to the output equation (2.2.4) as follows:

$$y_k = OCV(z_k) - s_k M(z_k) - R i_k \quad (2.3.1)$$

Where s_k represents the sign of the current (with memory during a rest period). For some sufficiently small and positive value ε, one has:

$$s_k = \begin{cases} +1 & i_k > \varepsilon \\ -1 & i_k < -\varepsilon \\ s_k - 1 & |i_k| \le \varepsilon \end{cases} \quad (2.3.2)$$

Also, note that $\mathrm{M}(\mathrm{z_k})$ is half the difference between the charge and discharge values (i.e., some value of hysteresis) [7]. Typically, the value for M can be assumed constant. As per [7], the zero-state hysteresis model is an improvement over the simple model, but only crudely approximates the underlying phenomenon. Whereas the level of hysteresis slowly changes as the cell is charged or discharged, the model estimates hysteresis as immediately flipping between its maximum positive and negative values when the sign of current changes.

D. One-State Hysteresis Model

The slow transition may be modeled by adding a 'hysteresis state' to the model. The hysteresis state is not a differential equation as a function of time, but in SOC (i.e., ampere-hours). Suppose that $h(z,t)$ is the hysteresis voltage, then one has [7]:

$$\frac{dh(z,t)}{dz} = \gamma sgn(\dot{z})[M(z,\dot{z}) - h(z,t)] \quad (2.4.1)$$

Where $\mathrm{M}(\mathrm{z},\dot{\mathrm{z}})$ is a function that gives the maximum polarization due to hysteresis as a function of SOC and the rate-of-change of SOC. The term $M(z,\dot{z}) - h(z,t)$ states that the rate-of-change of hysteresis voltage is proportional to the distance away from the main hysteresis loop; leading to a type of voltage decay in the major loop [7]. The term γ is considered positive and constant; and affects the rate of voltage decay [7]. The sign function forces the equation to be stable for both charge and discharge [7].

The overall state-space equations for the one-state hysteresis model are as follows [7]:

$$\begin{bmatrix} h_{k+1} \\ z_{k+1} \end{bmatrix} = \begin{bmatrix} F(i_k) & 0 \\ 0 & 1 \end{bmatrix} \begin{bmatrix} h_k \\ z_k \end{bmatrix} + \begin{bmatrix} 0 & 1 - F(i_k) \\ -\frac{\eta_i \Delta t}{C} & 0 \end{bmatrix} \begin{bmatrix} i_k \\ M(z,\dot{z}) \end{bmatrix} \quad (2.4.2)$$

$$y_k = OCV(z_k) - R i_k + h_k \quad (2.4.3)$$

Furthermore, note that $F(i_k) = \exp(-|\eta_i i(t) \gamma / C_n|)$.

E. Enhanced Self-Correcting Model

The enhanced self-correction (ESC) battery model represents one of the most accurate models that are currently being used for battery SOC estimation [7]. This model can accurately capture battery dynamics and thus can be implemented in a vehicle BMS as it accommodates for hysteresis, polarization time constants, and ohmic losses [7]. The ESC model in the state space form is as follows [7]:

$$\begin{bmatrix} f_{k+1} \\ h_{k+1} \\ z_{k+1} \end{bmatrix} = \begin{bmatrix} diag(\propto) & 0 & 0 \\ 0 & F(i_k) & 0 \\ 0 & 0 & 1 \end{bmatrix} \begin{bmatrix} f_k \\ h_k \\ z_k \end{bmatrix} + \begin{bmatrix} 1 & 0 \\ 0 & \left(1 - F(i_k)\right) \\ -\frac{\tau_i \Delta t}{C_n} & 0 \end{bmatrix} \begin{bmatrix} i_k \\ M(z,\dot{z}) \end{bmatrix} \quad (2.5.1)$$

$$y_k = OCV(z_k) - R i_k + h_k + G f_k \quad (2.5.2)$$

Where z_k is the state of charge, f_k is the states of the low pass filter on i_k which is used to characterize the polarization time constants, h_k is the state representing charging or discharging hysteresis effect, OCV is the open circuit voltage, C_n is the battery nominal capacity, R is the battery internal resistance, G is the output matrix of the low pass filter, and α are the poles of the low pass filter. This model contains two inputs as follows: i_k is the battery input current, and $M(z,\dot{z})$ which represents the maximum polarization due to hysteresis. The model has one output y_k, which is the terminal voltage. However, it is important to note that this model may be broken into two models; based on either two states or four states.

ESTIMATION STRATEGIES

A. Kalman Filter

In 1960, Rudolph Kalman presented a new approach to linear filtering and prediction problems, which would later become known as the Kalman filter (KF) [13]. The KF yields a statistically optimal solution for linear estimation problems in the presence of Gaussian noise. The KF is a model based method, derived in the time domain and a discrete-time

setting. A continuous-time version was developed by Kalman and Bucy, and is consequently referred to as the Kalman-Bucy filter [14]. Like many other filters, the KF is formulated in a predictor-corrector manner. The states are first estimated using the system model and input, termed as a priori estimates, meaning 'prior to' knowledge of the observations. A correction term is then added based on the innovation (also called residuals or measurement errors), thus forming the updated or a posteriori (meaning 'subsequent to' the observations) state estimates. The following five equations form the core of the KF algorithm, and are used in an iterative fashion. Equations (3.1) and (3.2) define the a priori state estimate $\hat{x}_{k+1|k}$ based on knowledge of the system A and previous state estimate $\hat{x}_{k|k}$, and the corresponding state error covariance matrix $P_{k+1|k}$, respectively.

$$\hat{x}_{k+1|k} = A\hat{x}_{k|k} + Bu_k \tag{3.1}$$

$$P_{k+1|k} = AP_{k|k}A^T + Q_k \tag{3.2}$$

The Kalman gain K_{k+1} is defined by (3.3), and is used to update the state estimate $\hat{x}_{k+1|k+1}$ as shown in (3.4). The gain makes use of an innovation covariance S_{k+1}, which is defined as the inverse term found in (3.3).

$$K_{k+1} = P_{k+1|k}C^T\left(CP_{k+1|k}C^T + R_{k+1}\right)^{-1} \tag{3.3}$$

$$\hat{x}_{k+1|k+1} = \hat{x}_{k+1|k} + K_{k+1}\left(z_{k+1} - C\hat{x}_{k+1|k}\right) \tag{3.4}$$

The a posteriori state error covariance matrix $P_{k+1|k+1}$ is then calculated by (3.5), and is used iteratively, as per (3.2).

$$P_{k+1|k+1} = (I - K_{k+1}C)P_{k+1|k} \tag{3.5}$$

The derivation of the KF is well documented, with details available in [13, 15, 16]. The optimality of the KF comes at a price of stability and robustness. The KF assumes that the system model is known and linear, the system and measurement noises are white, and the states have initial conditions with known means and variances [17]. However, the previous assumptions do not always hold in real applications. If these assumptions are violated, the KF yields suboptimal results and can become unstable [18]. Furthermore, the KF is sensitive to computer precision and the complexity of computations involving matrix inversions [19]. For nonlinear systems and measurements, the KF may be used to formulate the extended Kalman filter (EKF). In this case, the nonlinear system f or measurement h is linearized according to its Jacobian. Partial derivatives are used to compute linearized system and measurement matrices F and H, respectively found as follows [20]:

$$F_k = \left.\frac{\partial f}{\partial x}\right|_{\hat{x}_{k|k},u_k} \tag{3.6}$$

$$H_{k+1} = \left.\frac{\partial h}{\partial x}\right|_{\hat{x}_{k+1|k}} \tag{3.7}$$

Equations (3.6) and (3.7) essentially linearize the nonlinear system or measurement functions around the current state estimate [15]. This comes at a loss of optimality, as the KF gain is no longer considered to be the best solution to the estimation problem [16]. Note that the EKF process is the same as the KF process, except that (3.6) and (3.7) replace A and C, respectively.

B. Smooth Variable Structure Filter

The smooth variable structure filter (SVSF) was presented in 2007 [21]. The SVSF strategy is also a predictor-corrector estimator based on sliding mode concepts, and can be applied on both linear or nonlinear systems and measurements. As shown in Fig. 1, it utilizes a switching gain to converge the estimates to within a boundary of the true state values (i.e., existence subspace) [21]. The SVSF has been shown to be stable and robust to modeling uncertainties and noise, when given an upper bound on the level of un-modeled dynamics and noise [21, 22].

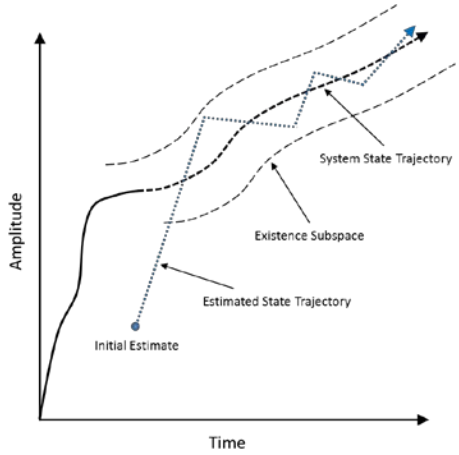

Fig. 1. The above figure shows the SVSF estimation strategy [23]. Starting from some initial value, the state estimate is forced by a switching gain to within a region referred to as the existence subspace.

The origin of the SVSF name comes from the requirement that the system is differentiable (or 'smooth') [21, 24]. Furthermore, it is assumed that the system under consideration is observable [21]. Consider the following process for the SVSF estimation strategy, as applied to a nonlinear system with a linear measurement equation. The predicted state estimates $\hat{x}_{k+1|k}$ are first calculated as follows:

$$\hat{x}_{k+1|k} = \hat{f}\left(\hat{x}_{k|k}, u_k\right) \tag{3.8}$$

Utilizing the predicted state estimates $\hat{x}_{k+1|k}$, the corresponding predicted measurements $\hat{z}_{k+1|k}$ and measurement errors $e_{z,k+1|k}$ may be calculated:

$$\hat{z}_{k+1|k} = C\hat{x}_{k+1|k} \tag{3.9}$$

$$e_{z,k+1|k} = z_{k+1} - \hat{z}_{k+1|k} \tag{3.10}$$

Next, the SVSF gain is calculated as follows [21]:

$$K_{k+1}^{SVSF} = C^{+}\left(\left|e_{z,k+1|k}\right| + \gamma\left|e_{z,k|k}\right|\right) \circ sat\left(\frac{e_{z,k+1|k}}{\psi}\right) \tag{3.11}$$

The SVSF gain is a function of: the a priori and a posteriori measurement errors $e_{z,k+1|k}$ and $e_{z,k|k}$; the smoothing boundary layer widths ψ; the 'SVSF' memory or convergence rate γ with elements $0 < \gamma_{ii} \leq 1$; and the linear measurement matrix C. The SVSF gain is used to refine the state estimates as follows:

$$\hat{x}_{k+1|k+1} = \hat{x}_{k+1|k} + K_{k+1}^{SVSF} \tag{3.12}$$

Next, the updated measurement estimates $\hat{z}_{k+1|k+1}$ and corresponding errors $e_{z,k+1|k+1}$ are calculated:

$$\hat{z}_{k+1|k+1} = C\hat{x}_{k+1|k+1} \quad (3.13)$$

$$e_{z,k+1|k+1} = z_{k+1} - \hat{z}_{k+1|k+1} \quad (3.14)$$

The SVSF process may be summarized by (3.8) through (3.14), and is repeated iteratively. According to [21], the estimation process is stable and convergent if the following condition is satisfied:

$$|e_{k|k}| > |e_{k+1|k+1}| \quad (3.15)$$

The proof, as described in [21] and [24], yields the derivation of the SVSF gain from (3.15). The SVSF results in the state estimates converging to the state trajectory. Thereafter, it switches back and forth across the state trajectory within a region referred to as the existence subspace. The existence subspace represents the amount of uncertainties present in the estimation process, in terms of modeling errors or the presence of noise. The width of the existence space β is a function of the uncertain dynamics associated with the inaccuracy of the internal model of the filter as well as the measurement model, and varies with time [21]. Typically this value is not exactly known but an upper bound may be selected based on a priori knowledge.

PSEUDO-INVERSE INSTABILITY

Numerous authors have experienced abrupt and unexpected instabilities with the pseudoinverse [25, 26]. A sudden growth of the Jacobian matrix elements when calculating the pseudoinverse during the SVSF gain calculation occurs at each epoch, as in (3.13). Consequently, the network's outputs and thus the mean squared error between the targets and outputs increase significantly. A stabilizing adjustment is performed to avoid this problem.

The problem has been extensively analyzed in [25], and occurs due to the presence of singularities. Singularities occur when the Jacobian matrix loses rank. Small singular values of C might arise in the vicinity of these singularities. Consequently, larger values ensue when obtaining the pseudoinverse of the Jacobian C^+ thus creating larger error values which leads to instability. According to [27], it is rather difficult to detect these singularities. A traditional method of solving this instability problem is to replace the pseudoinverse H^+ with the following equation:

$$C_d^+ = C^T(CC^T + \rho^2 I)^{-1} \quad (3.16)$$

Where, ρ is called the damping parameter. The effect of the added damping is that it mitigates the effect of small singular values when computing the inverse. Its disadvantage is that a small error is introduced when calculating the inverse [28].

BENCHMARK SIMULATION PROBLEM

In order to compare the abilities of the proposed models to capture the dynamics of a cell, data was gathered from the AVL CRUISE software platform. This software is a vehicle and powertrain simulation tool. The cell used in this study has a nominal capacity of 3.2 Ah and a nominal voltage of 3.5 V. The test involved an urban dynamometer driving schedule (UDDS) cycle used in AVL CRUISE. The vehicle velocity profile for the UDDS cycle is shown in Fig. 2. The corresponding battery pack current profile is shown in Fig. 3. For each model, the SOC as a function of time was captured, as well as the terminal voltage. A relatively large operating range was selected for the battery tests (20% to 80% of the SOC).

The mathematical relations that define the previous models have now been presented, but the constants numeric values to compare the models are necessary. The cell columbic efficiency factor was set to $\eta_i = 1$ for discharging and charging. The number of ampere-hours that can be drawn from the cell was set to approximately 3.2 Ah. The SVSF smoothing boundary layer was set to a constant $\psi = 100$ for the states and $\psi = 1 \times 10^{-2}$ for the parameters, and the SVSF convergence or 'memory' was defined as $\gamma = 0.1$. Note that these values were tuned by trial-and-error in an effort to reduce the estimation error.

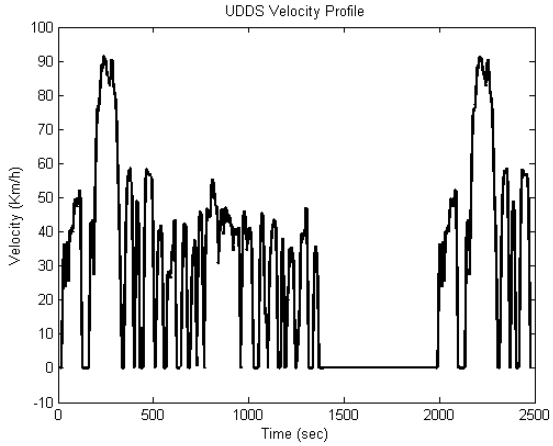

Fig. 2. Velocity profile for the UDDS cycle simulation. This set of data was used to test the models and compare the estimation methods.

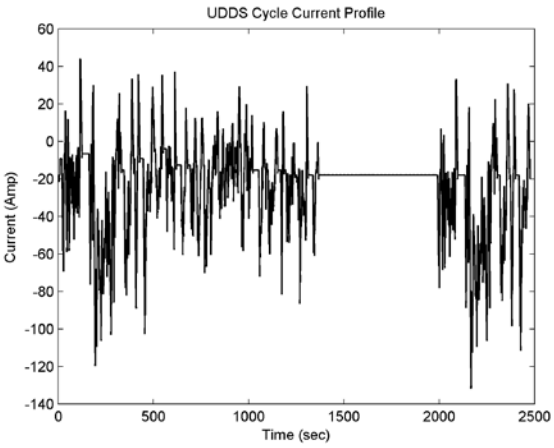

Fig. 3. Current profile for the UDDS cycle simulation. This set of data was used to test the models and compare the estimation methods.

The following series of figures were included for completeness, and include estimates for the SOC and voltage for each model. Following these figures, a summary of the root mean square error (RMSE) is provided.

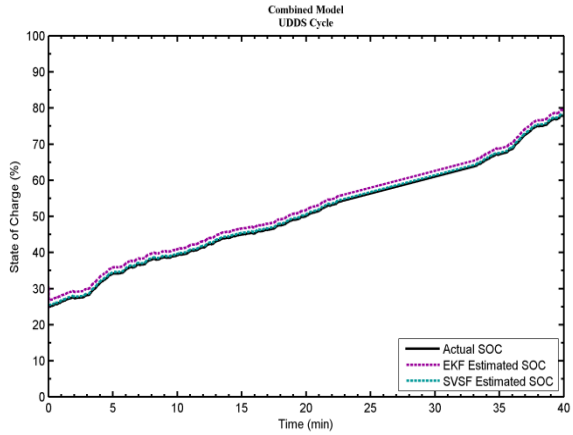

Fig. 4. Combined model results for the SOC. The actual SOC, and the estimated SOC (EKF and SVSF) are shown.

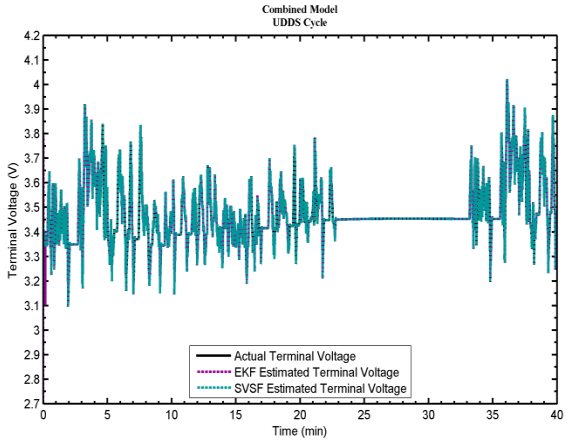

Fig. 5. Combined model results for the terminal voltage. The actual terminal voltage, and the estimated terminal voltage (EKF and SVSF) are shown.

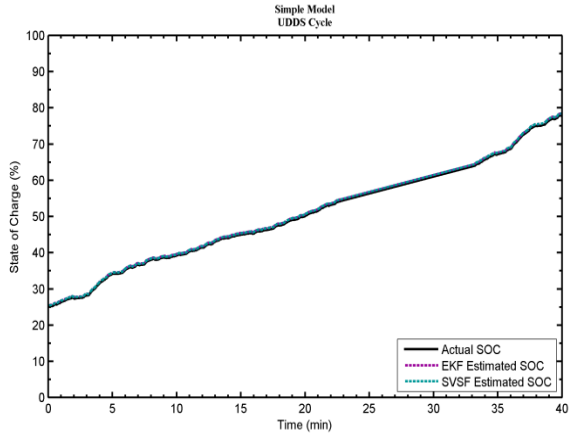

Fig. 6. Simple model results for the SOC. The actual SOC, and the estimated SOC (EKF and SVSF) are shown.

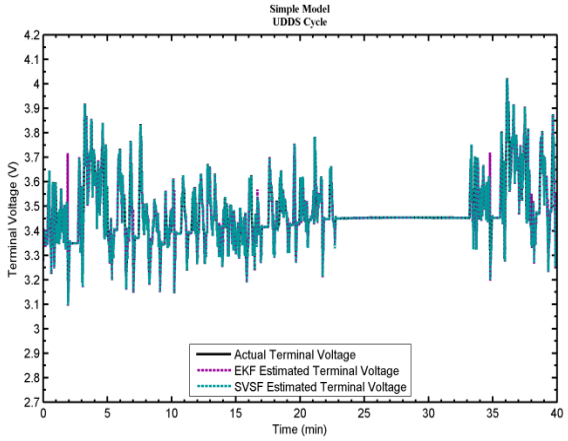

Fig. 7. Simple model results for the terminal voltage. The actual terminal voltage, and the estimated terminal voltage (EKF and SVSF) are shown.

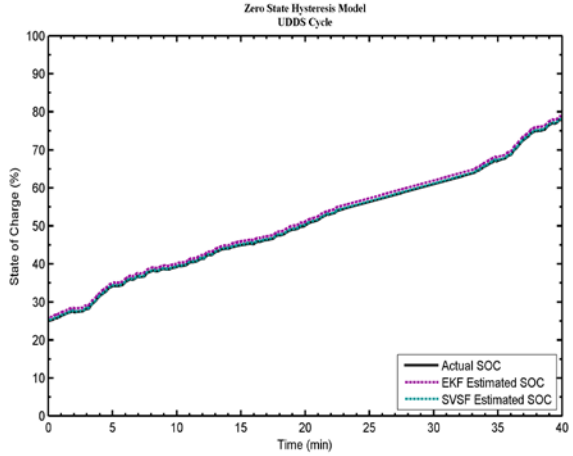

Fig. 8. Zero-state hysteresis model results for the SOC. The actual SOC, and the estimated SOC (EKF and SVSF) are shown.

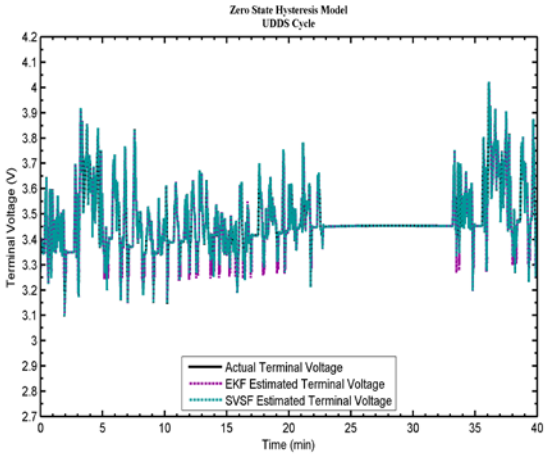

Fig. 9. Zero-state hysteresis model results for the terminal voltage. The actual terminal voltage, and the estimated terminal voltage (EKF and SVSF) are shown.

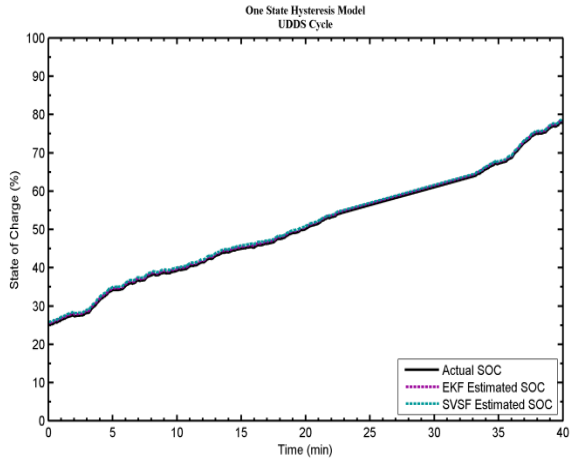

Fig. 10. One-state hysteresis model results for the SOC. The actual SOC, and the estimated SOC (EKF and SVSF) are shown.

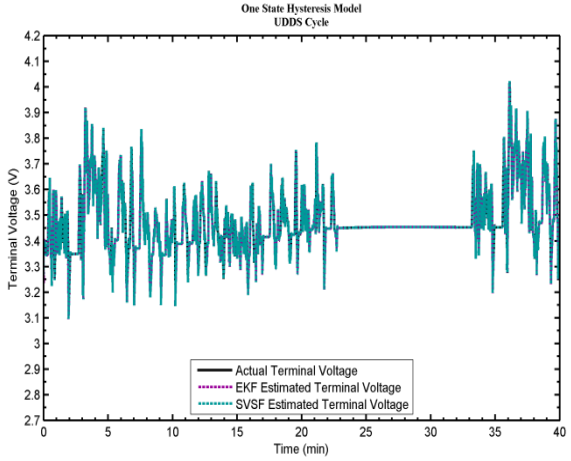

Fig. 11. One-state hysteresis model results for the terminal voltage. The actual terminal voltage, and the estimated terminal voltage (EKF and SVSF) are shown.

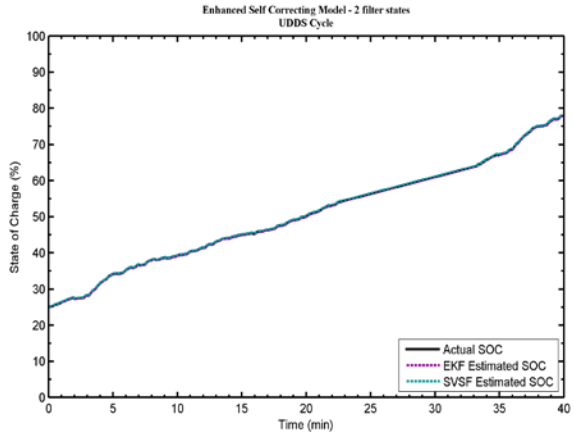

Fig. 12. Enhanced self-correcting model (two states) results for the SOC. The actual SOC, and the estimated SOC (EKF and SVSF) are shown.

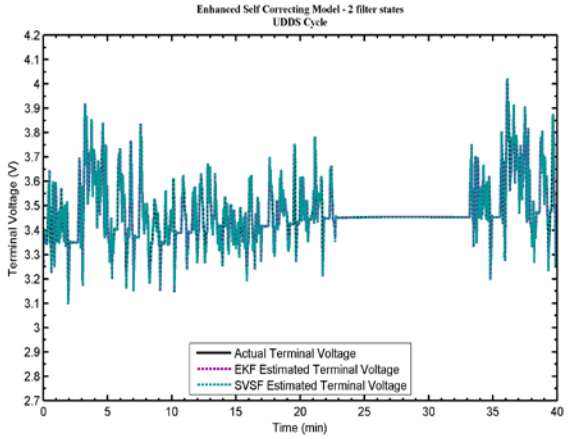

Fig. 13. Enhanced self-correcting model (two states) results for the SOC. The actual SOC, and the estimated SOC (EKF and SVSF) are shown.

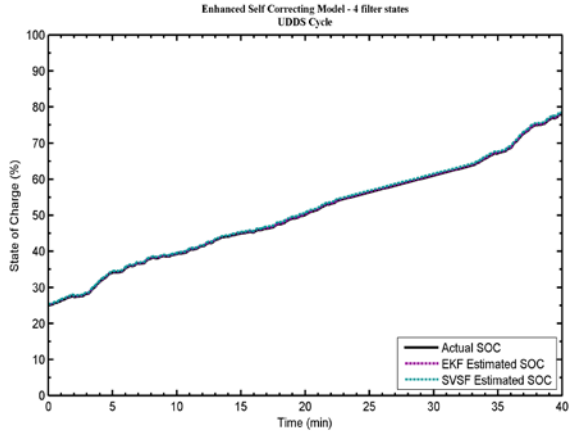

Fig. 14. Enhanced self-correcting model (four states) results for the SOC. The actual SOC, and the estimated SOC (EKF and SVSF) are shown.

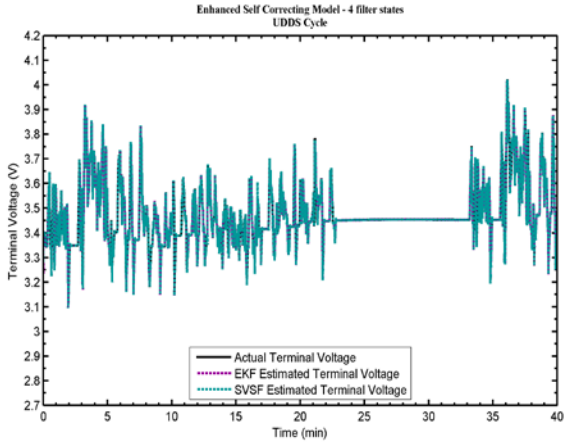

Fig. 15. Enhanced self-correcting model (four states) results for the SOC. The actual SOC, and the estimated SOC (EKF and SVSF) are shown.

The EKF requires values for the system and measurement noise covariance matrices, Q and R respectively. Although the papers [2, 7, 8] utilized the EKF, the authors omitted values for Q and R which makes reproducing results very difficult. In this paper, the measurement noise covariance was defined as $R = 0.01$. The system noise covariance matrix varied depending on which model was used. However, for the combined model, Q was defined as a diagonal matrix. For each state a value of $Q = 1 \times 10^{-6}$ was assigned, and for each parameter $Q = 5 \times 10^{-2}$ was implemented.

The following figure illustrates the RMSE results for the EKF and SVSF, as applied on the six different models. Note that the SVSF provides an improvement of 30% to 80% in terms of estimation accuracy. This is most likely due to the robust switching ability inherent in the SVSF gain. Note also that the SVSF was easier to tune when compared with the EKF. The EKF required a significant amount of tuning in terms of the Q and R elements, whereas the SVSF required only the SVSF boundary layer term to be tuned.

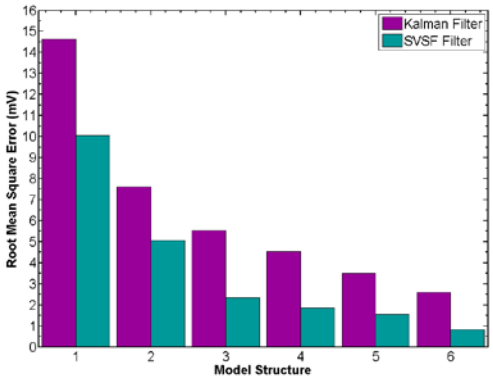

Fig. 16. Root mean square error (RMSE) results for the two filtering strategies applied on the six different models.

ACKNOWLEDGEMENTS

The authors would like to acknolwedge support from AVL for providing AVL CRUISE student licenses. The authors would also like to thank Mohammed El Sayed (Mechanical Engineering, McMaster University) for some help with the simulation.

CONCLUSIONS

The purpose of this paper was to compare the performances of some of the most popular Li-ion battery models found in literature. A benchmark dataset was used to study the effectiveness of these models. The extended Kalman filter (EKF) was applied for battery parameter estimation, and the results were compared with the smooth variable structure filter (SVSF). Overall, the SVSF provided better estimates in terms of estimation accuracy. Furthermore, the SVSF was easier to tune compared with the EKF. Although all of the models worked fairly well, the enhanced self-correcting model provided the most accurate battery model.

REFERENCES

[1] B. S. Bhangu, P. Bentley, D. A. Stone and C. M. Bingham, "Nonlinear Observers for Predicting State-of-Charge and State-of-Health of Lead-Acid Batteries for Hybrid-Electric Vehicles," *IEEE Transactions on Vehicular Technology,* vol. 54, no. 3, May 2005.

[2] G. L. Plett, "Extended Kalman Filtering for Battery Management Systems of LiPB-Based HEV Battery Packs: Part 1. Background," *Journal of Power Sciences,* vol. 134, no. 2, pp. 252-261, 2004.

[3] A. Vasebi, S. M. T. Bathaee and M. Partovibakhsh, "Predicting State of Charge of Lead-Acid Batteries for Hybrid Electric Vehicles by Extended Kalman Filter," *Journal of Energy Conversion and Management,* vol. 49, pp. 75-82, 2008.

[4] G. L. Plett, "Sigma-Point Kalman Filtering for Battery Management Systems of Li-PB-Based HEV Battery Packs: Part 1. Introduction and State Estimation," *Journal of Power Sources,* vol. 161, pp. 1356-1368, 2006.

[5] T. Okoshi, K. Yamada, T. Hirasawa and A. Emori, "Battery Condition Monitoring (BCM) Technologies About Lead-Acid Batteries," *Journal of Power Sources,* vol. 158, pp. 874-878, 2006.

[6] J. Voelcker, "Lithium Batteries Take to the Road," *IEEE Spectrum Magazine,* September 2007.

[7] G. L. Plett, "Extended Kalman Filtering for Battery Management Systems of LiPB-Based HEV Battery Packs: Part 2. Modeling and Identification," *Journal of Power Sources,* vol. 134, no. 2, pp. 262-276, 2004.

[8] G. L. Plett, "Extended Kalman Filtering for Battery Management Systems of LiPB-Based HEV Battery Packs: Part 3. State and Parameter Estimation," *Journal of Power Sources,* vol. 134, no. 2, pp. 277-292, 2004.

[9] J. Kim, S. Lee and B. H. Cho, "Complementary Cooperation Algorithm Based on DEKF Combined With Pattern Recognition for SOC/Capacity Estimation and SOH Prediction," *IEEE Transactions on Power Electronics,* vol. 27, no. 1, pp. 436-451, January 2012.

[10] X. Hu, S. Li and H. Peng, "A Comparative Study of Equivalent Circuit Models for Li-ion Batteries," *Journal of Power Sources,* vol. 198, pp. 359-367, January 2012.

[11] N. Nise, Control Systems Engineering, 4 ed., New York: John Wiley and Sons, Inc., 2004.

[12] K. Sakurai, K. I. Muramoto and T. Yamazaki, "Estimation of the Recharge Capacity of Sealed Lead-Acid Batteries by Neural Network," in *IEEE ITEC*, San Francisco, CA, 1998.

[13] R. E. Kalman, "A New Approach to Linear Filtering and Prediction Problems," *Journal of Basic Engineering, Transactions of ASME,* vol. 82, pp. 35-45, 1960.

[14] R. Kalman and R. Bucy, "New Results in Linear Filtering and Prediction Theory," *ASME Journal of*

Basic Engineering, vol. 83, pp. 95-108, March 1961.

[15] B. D. O. Anderson and J. B. Moore, Optimal Filtering, Englewood Cliffs, NJ: Prentice-Hall, 1979.

[16] A. Gelb, Applied Optimal Estimation, Cambridge, MA: MIT Press, 1974.

[17] D. Simon, Optimal State Estimation: Kalman, H-Infinity, and Nonlinear Approaches, Wiley-Interscience, 2006.

[18] S. J. Julier, J. K. Ulhmann and H. F. Durrant-Whyte, "A New Method for Nonlinear Transformation of Means and Covariances in Filters and Estimators," *IEEE Transactions on Automatic Control,* vol. 45, pp. 472-482, March 2000.

[19] M. S. Grewal and A. P. Andrews, Kalman Filtering: Theory and Practice Using MATLAB, 3 ed., New York: John Wiley and Sons, Inc., 2008.

[20] S. Haykin, Kalman Filtering and Neural Networks, New York: John Wiley and Sons, Inc., 2001.

[21] S. R. Habibi, "The Smooth Variable Structure Filter," *Proceedings of the IEEE,* vol. 95, no. 5, pp. 1026-1059, 2007.

[22] S. R. Habibi and R. Burton, "The Variable Structure Filter," *Journal of Dynamic Systems, Measurement, and Control (ASME),* vol. 125, pp. 287-293, September 2003.

[23] S. A. Gadsden, "Smooth Variable Structure Filtering: Theory and Applications," Hamilton, Ontario, 2011.

[24] M. Al-Shabi, "The General Toeplitz/Observability SVSF," Hamilton, Ontario, 2011.

[25] K. O'Neil and C. Y. -C, ""Instability of Pseudinverse Acceleration Control of Redundant Mechanisms," in *Proceedings of the IEEE International Conference on Robotocs and Automation*, April 2000.

[26] C. Melchiorri, C. Bonivento and K. Doty, "A theory oof generalized inverses applied to robotics," *International Robotics Journal,* vol. 12, pp. 1-19, 1993.

[27] H. Lipkin and E. Pohl, "Enumeration of singular configuration for robotic manipulators," *Journal of Mech. Design,* vol. 113, no. 3, pp. 272-279, 1991.

[28] R. Ahmed, "Training of Neural Networks Using the Smooth Variable Structure Filter with Application to Fault Detection," Department of Mechanical Engineering, McMaster University, April 2011.